A multiscale framework to estimate water sorption isotherms for OPC-based materials

A Multiscale Framework to Estimate Water Sorption Isotherms for OPC-based Materials

S. Babaei[*(1)a,b,c], S.C. Seetharam[(2)a], U. Muehlich[(4)b], A. Dizier[(5)c], G. Steenackers[(6)b,d] and B. Craeye[(6)b,e]

[a] Engineered and Geosystems Analysis Unit, Institute for Environment, Health, and Safety, Belgian Nuclear Research Centre (SCK•CEN), Boeretang 200, B2400 Mol, Belgium.

[b] Faculty of Applied Engineering, University of Antwerp, Groenenborgerlaan 171 - 2020 Antwerpen , Belgium

[c] EIG, EURIDICE, Belgian Nuclear Research Centre (SCK•CEN), Boeretang 200, B2400 Mol, Belgium

[d] University of Antwerp, Faculty of Applied Engineering | Op3Mech research group Groenenborgerlaan 171 - 2020 Antwerpen

[e] Odisee University College, Industrial Sciences & Technologies , DUBIT Research Unit, Belgium

(1)* Tel: +32 14 333125, saeid.babaei@uantwerpen.be; saeid.babaei@sckcen.be

(2) Tel: +32 14 333208, suresh.seetharam@sckcen.be

(3) Tel: +32 00 000000, uwe.muehlich@uantwerpen.be

(4) Tel: +32 00 000000, arnaud.dizier@euridice.be

(5) Tel: +32 00 000000, gunther.steenackers@uantwerpen.be

(6) Tel: +32 00 000000, bart.craeye@uantwerpen.be

ABSTRACT

This paper presents a new multiscale framework to estimate water sorption isotherms (WSI) for ordinary Portland cement (OPC) based materials. This is achieved by integrating: (i) particle packing, (ii) cement hydration kinetics, and (iii) pore network models. The first two models provide pore size distribution for gel and capillary pores. The pore network model takes these as inputs to construct an idealized network of pores connected by so called throats. By invoking appropriate thermodynamic equilibrium laws for the adsorbed and capillary water locally and using an existing percolation algorithm, WSI are estimated via a series of steady-state analysis. A notable feature of the proposed framework is that there is only one geometrical calibration parameter needed in the pore network model, excluding calibration inherent in the cement hydration kinetics model. The capability of the framework is demonstrated by comparing the model predictions with eleven independent experimentally determined WSI, in particular, desorption isotherms. It is shown that the model is able to estimate WSI with coefficient of determination (R^2) value being 0.85 or above for all the cases.

KEYWORDS

Cement hydration, Particle packing, Pore network, Multiscale, Concrete, Water sorption isotherm

1

1 INTRODUCTION

The importance of water content *vis-à-vis* the durability of cementitious materials is long established [1, 2]. In particular, water sorption isotherm (WSI) is a key material property that is used extensively in the study of moisture transport of unsaturated cementitious materials with a view to gain improved understanding of many durability problems such as drying shrinkage, creep, corrosion, carbonation, freeze-thaw, etc. The mechanisms affecting WSI are highly complex and depend on concrete composition such as cement type and content, water to cement ratio, aggregates, additives and fillers, moisture content and environmental factors such as ambient temperature [3].

A central theme of this study is to explore the possibility of going from the knowledge of mix composition to predicting WSI. Such a framework is of profound importance, for instance, in the study of durability of concrete structures in the existing nuclear power plants for which material properties such as drying shrinkage and creep are unknown. Hence, as far as possible, predictive approach to the determination of WSI is pursued so that any OPC based mixes can be accommodated without the need for an experimental campaign for every mix composition.

The principal approach to obtain WSI is via appropriate experimental techniques such as conventional wetting/drying [4, 5], dynamic vapour sorption [6, 7] and centrifuge experiments [8, 9]. For low permeability materials like cementitious materials, it is often time consuming to determine WSI accurately for the complete range of degree of saturation (S_w) [10]. However, once experimental data become available, an analytical model can be fitted in a way that WSI can be predicted for various conditions, for example, different water to cement ratios and porosity. An overview of such analytical models is available in Burgh et al. [11]; a notable work cited in their reference is that of Kumar et al. [12], which explored numerous analytical models to successfully predict WSI for a range of porosity. The accuracy of such models not only depend on their mathematical form but also on access to experimental WSI.

A second approach to predict WSI is to derive it from microstructural information such as pore size distribution and the type of water associated with different pore classes. Kelvin's equation is then used to establish an equilibrium relation between water content and capillary pressure, especially for gel and capillary pores. In this regard, Pinson et al. [13] predicted WSI by classifying water into interlayer, gel, capillary and surface adsorbed water. As a first approximation, they assumed a linear relationship between water content and capillary pressure for the interlayer space, i.e. for relative humidity below 15%. For the gel and capillary pores, they extracted pore size distribution from Barrett-Joyner-Halenda (BJH) method and then combined it with Kelvin's equation to derive WSI. For the empty pores in gel and capillary pores, they also considered the effect of adsorbed water via Langmuir and Brunauer–Emmett–Teller (BET) methods. Burgh et al. [11] proposed a model for WSI that also considers interlayer, gel and capillary pore classes as Pinson et al. [13]. They used a modified form of classic Powers and Brownyard hydration model [14] to capture pore volumes. Then a continuous probability distribution is used with shape and scale parameters calibrated with experiments to describe the whole pore size distribution range. With the pore size distribution, Kelvin's equation is used to determine the equilibrium relationship between water content and capillary pressure. More recently, Masoero et al. [15] studied the densification of Calcium-Silicate-Hydrate (C-S-H) gel and its effect on WSI during hydration. Their model combines a C–S–H gel description from nanoscale simulations with evolving capillary pore size distributions using a simple hydration model, however only for C_3S. This information is then coupled with Kelvin's equation to obtain WSI.

An interesting and alternative approach to predict WSI is the pore network model pioneered by Mason [16], which conceptualizes a porous material as a network of pores connected by throats (constrictions or windows) and locally invoking Kelvin's equation. He demonstrated the capability of the network model to predict adsorption-desorption hysteresis using a hypothetical

network. It was possible to capture hysteresis because pore blocking is a natural consequence of the network model where pore connectivity is inherently defined. In this regard, Islahuddin and Janssen [17] applied the pore network model to numerically explore WSI of Berea sandstone based on topologically equivalent network obtained from micro-CT scanning.

In conclusion, with the exception of Masoero et al. [15], the first two approaches strongly rely on experimental WSI for calibrating the model parameters before they can be used for predictions. Although, Masoero et al. [15] do not use experimental WSI, their model is demonstrated for C_3S (Alite) system only. In addition, the first two approaches will need some calibration to incorporate sorption hysteresis unlike the alternative approach. Finally, to the authors' knowledge, the alternative approach, i.e. the pore network model has never been applied to complex microstructures such as cementitious materials. Although the pore network model is applied for other porous materials, it relies entirely on experimental pore size distribution as a key input.

This study therefore proposes a new framework to estimate WSI via a multiscale approach, which integrates particle packing, cement hydration kinetics and pore network models. Thus no experimental data concerning pore size distribution or WSI (except for geometrical parameter) is needed as inputs other than the composition of the material, known microstructural features of high density (HD) and low density (LD) C-S-H phases for OPC based materials and cement hydration kinetics model, which is usually calibrated with hydration experiments. The capability of the framework is demonstrated by comparing the model predictions with a number of experimental desorption WSI. Desorption WSI has been the focus because the ultimate goal of the present study is oriented towards drying shrinkage problems within the context of unsaturated poroelasticity.

2 MULTISCALE FRAMEWORK

The proposed multiscale framework for water sorption isotherm integrates three models: (i) cement particle packing, (ii) microstructural cement hydration kinetics, and (iii) pore network. For lower (gel) pore size range, which is characterized by HD and LD C-S-H, the particle packing model computes total porosity and pore size distribution relying on a principal assumption that the variability of HD and LD C-S-H characteristics in terms of particle packing is limited for OPC [18]. Based on fundamental inputs such as cement composition and reaction conditions, the microstructural model computes volume fractions of various hydrated phases, capillary porosity and pore size distribution but for a higher capillary pore size range (> 1 μm), which is primarily dictated by the limitation of resolution of the model used. However, these two models do not cover the mid pore size range (small capillary pores), i.e. between tens of nm to 1 μm, as demonstrated in *Figure 1*. Therefore, an approximation to cover this missing pore size range is proposed (Section 2.3) and justified (Section 3). Based on the computed pore size distribution for the full range of pore sizes, the pore network model computes WSI for a given material composition. These steps are illustrated in *Figure 2*.

2.1 PARTICLE PACKING MODEL: nm scale

In order to estimate porosity and pore size distribution of lower (gel) pore size range, a conceptual model that describes the microstructure of C-S-H gel has to be chosen. Various conceptual models such as layered, colloidal and fractal models have been proposed in the recent past [19]. The particle packing model used in this study follows the colloidal model for C-S-H gel proposed by Jennings [20] and illustrated in *Figure 3*. This is a self-consistent model with respect to a number of experimental data, for example, specific surface area and density measurements. The term ‘particle’ used in this study equates to the term ‘C-S-H globules’ in the Jennings’s model. These globules (particles) are packed together to form HD and LD C-S-H and the spacing between the globules are referred to as gel pores. Thus if the packing density

for HD and LD C-S-H are known then their respective gel porosities as well as pore size distribution can be geometrically extracted. However, the pore size distribution of pores larger than the gel pores cannot be estimated with the particle packing model. Some assumptions are made to fill this missing information as discussed in Section 2.3.

The two types of C-S-H phases, namely, HD C-S-H and LD C-S-H are well-characterized [21-23]. The difference between the two C-S-H phases mainly lies in their gel porosity and packing density; the HD C-S-H being characterized by a gel porosity, φ_{HD}, of roughly 0.24, and the LD C-S-H being characterized by a gel porosity, φ_{LD}, of roughly 0.37. It is worth noting that the corresponding packing densities, $(1 - \varphi_{HD}) = 0.76$ and $(1 - \varphi_{LD}) = 0.63$, come very close to the maximum packing densities of mono-sized spherical packing. The packing density of HD C-S-H is of striking similarity to the highest possible density of ordered spheres, known as the face-centred cubic lattice, equal to 0.74, and the packing density of the LD C-S-H is of striking similarity to the so-called random close packing (RCP) of 0.64 [24-27].

The particle packing model used in this study is similar to the work of Fonseca et al. [19] and Liu et al. [28]. The choice for the size of the particles is based on Jennings's [20] conceptual model, which considers mono-sized particles of size 5.6 nm (*Figure 3*). With respect to pore size distribution, a representative volume element (RVE) of size 150×150×150 nm^3 is chosen after testing three different RVE sizes (100 nm, 150 nm and 200 nm). Liu et al. [28] also arrived at the same RVE size after testing various RVE sizes. So, Initially, a small number of mono-sized particles each of diameter 5.6 nm are randomly distributed in space, and then they are compacted to the maximum extent without overlapping by moving spheres closer to the centre of the RVE. A new set of particles is added and again compacted. This procedure is repeated until the desired packing density is achieved. One additional step that is taken in comparison to the work of Liu et al. [28] is that after compacting, the compacted globules are further discretized into sub-globules made of mono-sized spheres with size of 2.2 nm, so that the water

in the interlayer space (space between 2.2 nm spheres) are also accounted to be consistent with the Jennings' colloidal model. With this, the extraction of pore size distribution is carried out (*Figure 3*). The results obtained from this model corresponds well with the model of Liu et al. [28] for HD C-S-H as shown in *Figure 4*, which is attributed to the fact that the maximum density has to be achieved irrespective of the algorithm used. However, there is some deviation for LD C-S-H, which is attributed to the fact that the required packing density is lower compared to HD C-S-H, which means the results can become sensitive to the particle packing algorithm and pore size distribution extraction method. It is also worth noting that typically 40% of the total volume of RVE of cement paste is comprised of HD and LD C-S-H [1]. Therefore, the particle packing model accounts for majority of the pore size range.

2.2 MICROSTRUCTURAL CEMENT HYDRATION KINETICS MODEL: μm scale

All the existing microstructural models are mainly intended to study microstructural properties such as volume fractions of hydrated phases, porosity, percolation threshold and degree of hydration but not pore size distribution. There are currently no cement hydration kinetics models that can estimate reliable pore size distribution. This is a limitation of this framework. However, as a first approximation, such a hydration kinetics model is still relied upon for estimating pore size distribution.

A comprehensive review of microstructural modelling and in particular cement hydration kinetics models can be found in Thomas et al. [29]. From the latter as well as author's own experience, it is found that Virtual Cement and Concrete Testing Laboratory (VCCTL) suite offers control over wide range of variables and input parameters and is experimentally better validated compared to other hydration models [30]. Hence, VCCTL is taken forward in this study. In VCCTL, a 3D cement paste microstructure is digitized into a cubic lattice and each volume element or voxel of the cube is assigned to a phase (porosity, C-S-H, CH, etc.). VCCTL

simulates the hydration process as an iterative procedure of dissolution, diffusion, and reaction. This iteration evolves the initial lattice cube and forms a reasonable spatial distribution of the anhydrite cement, combined hydration products, and capillary porosity. The minimum voxel size that can be specified is 1 μm, which also implies that capillary pores below 1 μm cannot be captured. Hence, only total porosity and pore size distribution of pores greater than 1 μm can be captured.

Note that one may also consider cement hydration kinetics model that are resolution free or vector-based (e.g. HYMOSTRUC [31]), which have no limitation on the minimum voxel size. However, as shown by Ye [32], the modelled pore size distribution results are not promising. Such resolution free microstructural models are usually used with voxel size larger than 1 μm, as capturing the hydration and interaction of the cement particles from nano to micro scale is computationally prohibitive. Moreover, such resolution free models read the spaces existing between the reaction products but not the pores within the C-S-H gel as a product of hydration reaction [33]. This in fact justifies the use of particle packing (Section 2.1) as a necessary component of the framework to estimate gel pore size distribution.

2.3 MISSING PORE SIZE DISTRIBUTION: nm to μm scale

The missing pore size distribution from biggest gel pores (14 nm based on particle packing) to smallest capillary pore imposed by the hydration model (1 μm by VCCTL) is derived by using the pore size distribution of the capillary pores as a surrogate (Section 2.2). In the absence of any data, this should be treated as a crude approach. The implication of this approximation is discussed in Section 3.1. In this approach, a Weibull distribution function is fitted on the capillary pore size distribution obtained from VCCTL, which is available from one μm to tens of μm. The Weibull distribution function is defined as:

$$f(x) = \frac{\beta}{\eta}\left(\frac{x-\gamma}{\eta}\right)^{\beta-1} e^{\left(\frac{x-\gamma}{\eta}\right)^{\beta}} \quad (1)$$

where x is a pore size, β is the shape factor, η is the scale parameter and γ is the location parameter. Once the Weibull distribution is fitted for the capillary pore size range, the shape is preserved but by manipulating the location and scale parameter the pore size range is stretched to cover a wider range from 14 nm to 1 μm. This missing pore size range is then added to the capillary pore network, ensuring that the calculated capillary porosity is still respected.

2.4 PORE NETWORK MODEL

The estimation of WSI of cementitious material is carried out using a pore network model with steady state analysis. A pore network is a virtual network of pores and throats, which are connection between the pores [34]. This model can reconstruct WSI on the whole capillary pressure range provided accurate pore/throat size distribution data as well as topology of the network are available, including appropriate physics given the pore size range of a typical cement paste material.

There are several techniques to characterize the pore space. Imaging techniques such as producing 3D images by mapping the real interior structure of original material are promising but time consuming and expensive. This mapping can be carried out using destructive approach of cutting and stacking serial 2D sections, followed by confocal laser scanning microscopy, non-destructive X-ray micro-tomography (μCT), and constructing synthetic 3D images from high resolution 2D thin sections using statistical methods or geological process simulation [34, 35]. However, as already described in Sections 2.1 and 2.2, in this study, pore space is characterized based on the particle packing and available microstructural modelling tools (VCCTL here).

In this study, the pore space of the cementitious material is characterized by means of three main networks: HD C-S-H, LD C-S-H and capillary porosity. The most important variable to

construct a network in this regards is the volume fractions of these three networks. First of all, the volumetric ratio of HD and LD C-S-H network is estimated via Jennings-Tennis's hydration model [36]. Depending on this ratio, the porosity of the whole gel pore space is derived as follows:

$$\varphi_{gel} = \varphi_{HD}.V_{HD} + \varphi_{LD}.V_{LD} \quad (2)$$

where φ_{HD} is the porosity of HD C-S-H equal to 0.24 [21], V_{HD} is the volume fraction of HD C-S-H in C-S-H gel, φ_{LD} is the porosity of LD C-S-H equal to 0.37 [21], and V_{LD} is the volume fraction of LD C-S-H with $V_{HD} + V_{LD} = 1$.

The volume of gel pores is defined as:

$$V_{gel} = V_{CSH}.\varphi_{gel} \quad (3)$$

where V_{CSH} is the volume fraction of C-S-H gel, which is obtained from the hydration model (section2.2). The volume of capillary pores is also obtained from the hydration model. Once the volume fractions of all the networks are available, a unified network can be generated by merging all these three networks. Each network has its own pore size distribution and size, which comes from the hydration model, particle packing model and aforementioned equations.

2.4.1 GEOMETRICAL CONSIDERATIONS

To ensure that the simulations are reproducible, which means keeping fitting coefficients to a minimum (Eq. (4) and (5)), and to avoid convergence problem, a cubic network with fixed coordination number is constructed for each phase, i.e. HD C-S-H, LD C-S-H and capillary porosity. The pores and throats of the network can have different geometries such as cubes, triangles, spheres, cylinders, etc. To accelerate the simulation, in this study, the pores are defined as spheres and throats as cylindrical pipes. To construct a cubic network of specific size, in addition to pore size, the connectivity or coordination number and throat sizes and lengths are required. The coordination number is defined as the number of connected throats

for each pore. Real porous materials might have different coordination numbers based on their pore structure but to optimize the simulation procedure, the coordination number of the cubic network is taken as six. This means each pore is connected to its six neighbouring pores. *Figure 5* demonstrates a few examples of networks with coordination numbers of 6, 12 and 26 for a network with 27 pores.

It is not possible to experimentally obtain throat size distribution as the network of pores and throats are idealization of complex pore network in cementitious materials. Hence, some assumptions have to be made. The first rule to define throat size is to make sure that every throat diameter is smaller than its neighbouring pores. As a first approximation, the throat size, R_{throat}, is arbitrarily defined as a linear function of the radius of neighbouring pores, R_{np} as follows:

$$R_{throat} = \alpha\left(\min\left(R_{np}\right)\right) \quad (4)$$

where α is a factor whose value should be less than 1. For instance, for a configuration of three pores A, B and C shown in *Figure 6* with radius $R_a \leq R_b \leq R_c$, the throat size for their connecting throats should be:

$$R_{ab} = \alpha R_a,\ R_{bc} = \alpha R_b \quad (5)$$

It is also worth mentioning that the throat length is also defined using a comparable equation as Eq.(5), where the length of the connecting throat between two pores is defined as:

$$L_{throat} = \beta\left(max\left(R_{np}\right)\right) \quad (6)$$

with β being a scaling factor, which should be greater than 1 so that there is no overlapping of pore neighbouring pore bodies. In this study, the following values have been assigned to the coefficients: $\alpha = 0.3$ and $\beta = 1 + \alpha$. The α value is calibrated with an arbitrary WSI (experimental WSI presented in Section 3.2) and is held constant.

244 The following procedure is adopted to generate the overall pore network geometry:

245 a) Assuming that the volume fraction of LD C-S-H is higher than HD C-S-H, the first step
246 in the network construction is to generate an LD C-S-H network as a cubic network of
247 100 pores on each side of the cube, distributed within a 200×200×200 μm^3 RVE. Since
248 capillary pores, which are usually bigger (up to tens of μm) than the gel pores, are added
249 to the same RVE, the RVE dimensions are considered slightly larger than is necessary
250 for solely gel pores.
251 b) The second step is to generate the HD C-S-H pores and embed them inside the cubic
252 LD C-S-H network until their volume fraction reaches a certain ratio to LD C-S-H
253 volume fraction estimated from the hydration model (*Figure 7*(a)). This is achieved by
254 embedding the HD pores (grey) between the LD pores (green) as illustrated in the inset
255 of *Figure 7*(a). This step should also ensure that the ratio of HD to LD C-S-H as
256 estimated from the Jennings-Tennis's model is respected. It is worth mentioning that
257 during this merging process the coordination number is continuously checked and if
258 necessary throats are trimmed to meet the coordination number of six for the overall
259 network. Furthermore, note that the HD C-S-H can be as big as the LD C-S-H network
260 or even bigger than the LD C-S-H network depending on its volume fraction. If they are
261 of the same size, it does not matter, which network is constructed first. The sequence
262 should however be reversed in case the HD C-S-H network is larger than the LD C-S-
263 H network. It is worth noting that, by merging these two networks the homogenized C-
264 S-H network will result in a WSI, which falls between the pure HD C-S-H and LD C-
265 S-H networks as illustrated in *Figure 8*.
266 c) The first two steps yield a homogenized C-S-H gel network into which the capillary
267 pore network is embedded in the third (final) step. The capillary pores are added in a
268 different manner compared to the C-S-H pores. Since in terms of number of pores the

capillary pores have the smallest population and to avoid over estimation of ink-bottle effect, these pores are randomly distributed in the network rather than starting from the centre. Hence, as shown in *Figure 7*(b), capillary pores (red) can be spread anywhere in the central region and beyond within the homogenized C-S-H network (grey and green). If the RVE is sufficiently large then the randomness of the capillary pores should not significantly influence the WSI.

It is important to note that from the point of view of pore network geometry, RVE basically implies that the domain is sufficiently large enough to cover the entire pore size range as well as to ensure that the random distribution of pores do not significantly affect WSI (converged solution). RVE does not necessarily correspond to the actual RVE size because of the idealization involved in the representation of pores and throats.

2.4.2 WATER SORPTION ISOTHERM

Because of a large variation in pore sizes and their topological arrangement in low permeability materials as is the case with hardened cement paste, a WSI displays hysteresis [37]. In the case of cement paste, this behaviour can be attributed to irreversible processes such as morphological changes in microstructures, cracking or ink-bottle effect. Both adsorption and desorption WSI are of interest to understand the moisture transport behaviour of the material as well as for moisture transport modelling. In this paper, specific attention is paid to estimating desorption isotherms because of its direct relevance to the study of drying shrinkage behaviour and issues. Desorption isotherm also implies that some sort of invasion algorithm is necessary to mimic desorption of the initially saturated pore network.

In this study, an idealized pore network is generated using an in-house code developed in the SciPy and NumPy environment. The OpenPNM [34] library is then called upon to compute desorption isotherms. The OpenPNM library uses an “invasion percolation” algorithm based

on the work of Wilkinson and Willemsen [38]. However, additional considerations concerning adsorbed water are introduced. The invasion of moist air will occur only if the applied capillary pressure (external *RH*) exceeds the entry pressure of a pore/throat, which is calculated using the Young-Laplace's equation:

$$P_C = \frac{2\sigma \cos(\theta)}{r} \quad (7)$$

where σ is the surface tension (N/m), θ is the contact angle (°), and r is the pore radius (m) of a given pore/throat, which comes from the pore/throat size distribution. Since water perfectly wets the silicate materials and the presence of surface adsorbed water is taken into account, the contact angle is set to zero in this study [17, 39].

The invasion algorithm works in such a way that the pores with lowest entry pressure is first invaded. The throats that are connected to the invaded pores then become accessible and thus join the invasion front. This procedure is repeated until all the pores/throats are completely invaded. Further details of the algorithmic implementation are available in Gostick et al. [34] and references therein.

The invasion of pores/throats by moist air (external *RH*) does not imply that all the liquid water is completely evacuated from them because water may still be present in the form of absorbed water, which is in equilibrium with the local relative humidity, h_m. Hillerborg [40] defined absorbed water as sum of adsorbed and capillary condensation water. He attempted to propose a relationship between h_m and the radius of curvature of absorbed water by combining the standard Kelvin and Young-Laplace equations. However, as it was difficult to define the curvature of the absorbed water surface, as an approximation, only the curvature of adsorbed water was considered, which was determined based on the thickness of adsorbed water, t, via:

$$t = \frac{0.525\times10^{-8} RH}{(1-{RH}/{h_m})(1+{RH}/{h_m}+15RH)} \quad (8)$$

where RH is the external relative humidity (boundary condition) and h_m is defined via:

$$h_m = exp\left(\frac{-2\sigma}{R_v T(r-t)}\right) \quad (9)$$

where R_v is the gas constant of water vapour (J/kg/K), T is the temperature (K) and r is the radii of pores/throats. Note that Eq. (8) is a modification of the conventional BET model proposed by Hillerborg [40] to account for changes in h_m.

To quantify pore wetting/drying mechanism in the pore network model, P_c is considered as the primary variable. An illustration of simulation of free drying of a cube of cement paste using the pore network model is shown in *Figure 9*. In order to mimic real experimental conditions, the pore network is assumed to be initially saturated (P_c=0) and a constant boundary condition of P_c>0 (or RH<1) is prescribed incrementally over the entire RH range (0 to 1). This condition initiates drying of pores and throats until thermodynamic equilibrium is reached between the network and the prescribed external P_c based on the invasion percolation algorithm. The equilibrium S_w is then computed by taking the ratio of volume of elements of pore network that are still wet and the total volume of the network. Adsorbed water (if present) in the pores/throats is also accounted for in the calculation of S_w. Note that the entire computation is purely a steady state analysis for each increment of P_c.

3 VALIDATION

The proposed framework is validated against a wide range of measured desorption isotherms available in literature [10, 41-45]. The chosen datasets include plain cement paste, mortar and concrete to examine the capability of the modelling framework to handle different cementitious materials. The W/C of these materials varies from 0.34 to 0.8. The mineral composition and a short description on preparation and measurement methods of the studied cases are presented in *Table 1*. Further details of the experiments can be found in [10, 41-45].

Recall from Section 1 that the ultimate goal of the present study is oriented towards understanding of drying shrinkage problems within the context of unsaturated poroelasticity (e.g. [46]), where WSI is a key input data. In unsaturated poroelasticity, apart from S_w, the primary variable is typically capillary pressure instead of relative humidity (RH), which is measured experimentally. Therefore, all experimental RH data used in this study are converted to capillary pressure via Kelvin's equation, which is assumed to be valid irrespective of microstructure or RH.

The hydration model considers appropriate curing conditions, including temperature as reported in Table 2. In particular, the curing period varies from 56 days to 1 year at which time the rate of change of degree of hydration is expected to be minimal. Accordingly, variations in pore size distribution or porosity is also considered to be minimal and hence neglected beyond the curing period. Similarly, the pore network model considers laboratory temperature reported in Table 2 in order to correctly interpret temperature dependent RH changes.

3.1 INFLUENCE OF CAPILLARY PORES

Recall from Section 2.3 that a crude approach was proposed to account for the missing capillary pore size distribution in the range 14 nm to 1 μm. To justify this approach, the influence of capillary pore size range on WSI is examined in this section with the help of a series of virtual

358 experiments. A network including C-S-H gel pores with evenly distributed HD and LD pores
359 (50% HD C-S-H, 50% LD C-S-H) is generated, following which a capillary network is added.
360 Influence of variation of the mean pore size of the added capillary network and its volume
361 fraction are then studied. The volume fraction of the capillary network varies from 40% of the
362 total porous phase (Eq.1-2) to 70% and four different mean pore sizes are considered: 0.1 μm,
363 0.5 µm, 1 μm and 10 μm. The predicted WSI for such networks with 40%, 50%, 60% and 70%
364 of volume fraction of capillary porosity is presented in *Figure 10*.

365 It is seen that as the volume fraction of capillary porosity increases, the effect of its pore size
366 range becomes slightly more pronounced. For example, the network with 40% capillary pores
367 and mean capillary pore size of 10 μm has a maximum deviation of 6% compared to a network
368 with mean capillary pore size of 0.1 μm. Whereas, the same comparison for a network with
369 70% capillary pores has 9% deviation. Although the difference of 3% does not seem to be a big
370 deviation, these networks are constructed in an ideal sense where the proportion of HD and LD
371 C-S-H is fixed. In reality, higher porosity means either higher W/C or lower hydration degree
372 and consequently higher percentage of LD than HD C-S-H, which shifts the whole retention
373 curve.

374 However, an important conclusion from *Figure 10* is that the capillary pore size distribution
375 and capillary pore size range (> 14 nm) do not significantly affect WSI. At least three reasons
376 can be attributed to this insensitivity:

377 a) The population of capillary pores are at least two orders of magnitude lower than gel
378 pores to have any pronounced effect. For example, for the material CP5, the calculated
379 volume fraction of C-S-H gel is 47% (of which 72% is LD and 28% is HD C-S-H) and
380 that of capillary porosity is 37% (*Table 2*). The 47% C-S-H gel fraction with
381 aforementioned LD and HD C-S-H ratios results in 13% of LD C-S-H gel pores and 3%
382 of HD C-S-H gel pores. This distribution results in 1 million LD C-S-H pores and 1.28

383 million HD C-S-H pores. In contrast, the calculated capillary pores are only 23,552 in
384 the total pore space.

385 b) From Eq. (10), the relative humidity at which a pore radius of 20 nm (T=293 K) is
386 invaded is 0.95. Whereas, a big capillary pore with a radius of 10 μm is invaded at a
387 relative humidity of 0.99. Because of this narrow range of relative humidity covering
388 the whole range of capillary pores, the invasion sequence is not considerably affected
389 to significantly influence WSI.

390 $$r_p = -\frac{2\gamma}{\left(\frac{RT}{M}\right) ln\, RH} \quad (10)$$

391 c) In addition, because of the random distribution of capillary pores as well as its smaller
392 population in the overall pore network, the invasion sequence is not considerably
393 affected. For example, not all the capillary pores are exposed to air once the relative
394 humidity reaches 0.95 because some of them are trapped between the gel pores.

395 Therefore, the crude approach proposed in Section 2.3 to handle the missing pore size
396 distribution in the pore size range of 14 nm to 1 μm is justified, at least for predicting WSI.

397 ## 3.2 WSI PREDICTIONS

398 Based on the material composition defined in *Table 1*, predicted phase fractions of C-S-H and
399 the porosity of LD C-S-H, HD C-S-H and capillary pores are presented in *Table 2*, which form
400 basic inputs for generating pore networks. The results show that the capillary porosity and
401 volume fraction of LD C-S-H increase with increase in W/C and the volume fraction of HD C-
402 S-H shows opposite trend (Table 2). The results also show that the capillary porosity of cement
403 paste is larger than that of concrete for the same W/C. All these are qualitatively consistent with
404 the known behaviour of OPC [37].

405 *Figure 11* to *Figure 13* show comparisons of experimental WSI against the pore network model
406 results for the materials mentioned in Table 2. It is seen that for all materials the model provides
407 reasonably good correlation. The accuracy in the lower saturation regime is considerably higher
408 than the rest of the curve, revealing that the C-S-H gel has a reproducible behaviour and its
409 variation is more limited than capillary pores. However, there are some deviations for materials
410 CP2, Co1 and Co2, which may be attributed to uncertainties in the composition of the materials
411 used in the experiments as well as the idealizations and assumptions in the particle packing and
412 pore network model. Nevertheless, it is reasonable to conclude that the particle packing model
413 provides reliable inputs for pore network modelling.

414 For the materials CP1, CP3, CP5, M2, Co1 and Co2, the model slightly underestimates WSI in
415 the mid-range saturation regime. Part of the reasoning is the same as mentioned above for lower
416 S_w, but in addition, the reliability of the pore size distribution extracted from the hydration
417 kinetics model is also a major factor. Recall from Section 2.2 that the existing hydration kinetics
418 models are not intended to capture pore size distribution and is admitted only as a first
419 approximation in this study.

420 Furthermore, note that CP5 and M2 are from the same dataset where a standard for cement type
421 used is reported but XRD information of the chemical composition is not available. Co1 and
422 Co2 are concrete (cement paste + aggregate) and the ability of hydration models to account for
423 the presence of aggregates is yet to be examined. Finally, CP1 is a one year old sample, which
424 means self-desiccation would have occurred, which is not considered in the present framework.
425 The above issues add further uncertainties, which are reflected in the marginal deviations
426 observed in the predicted WSI.

427 Table 3 shows that R^2 value (coefficient of determination [47]) is 0.85 or above for the studied
428 cases. Given the available tools and assumptions, the overall performance of the multiscale
429 framework is highly encouraging.

4 CONCLUSIONS

A largely predictive multiscale framework for the estimation of WSI is proposed. This is achieved by integrating the following models: (i) particle packing, (ii) cement hydration kinetics, and (iii) pore network. The need for predicting pore size distribution necessitates the use of particle packing and cement hydration models, including Jennings-Tennis's model to obtain additionally the HD-LD C-S-H ratio. Based on the predicted (complete) pore size distribution of the material, the merging of HD C-S-H, LD C-S-H and capillary pore networks has been proposed, which actually leads to a very large pore network with few millions of pore bodies and throats. Both capillary water and adsorbed water are considered in estimating water content for WSI calculations. The pore network is implemented in the SciPy and NumPy computational environment with recourse to an existing library called OpenPNM, which uses an efficient invasion algorithm. A quasi-static analysis of the network using Kelvin's equation is then invoked in pore bodies and throats to estimate desorption WSI, the latter because the ultimate goal of this study is to address drying shrinkage problem.

The capability of the framework has been demonstrated with eleven independent experiments available from literature. A reasonably good correlation with experimental WSI has been demonstrated for all the experiments, with deviations explained. In fact, the R^2 value is equal to or above 0.85 for any of the comparisons. It is important to note that calibrations primarily stem from the cement hydration kinetics and Jennings-Tennis's model, which are usually based on hydration experiments for OPC based materials. Secondly, for the particle packing model, the knowledge of the particle size and packing density is required, which also comes from experimental investigations. From the pore network model perspective, only one calibration parameter exists, which is related to the throat size, and can be calibrated on any one experimental WSI. This framework therefore allows a greater flexibility to study WSI behaviour of arbitrary OPC based materials. Note that if experimental pore size distribution is

455 available then the pore network model is solely sufficient to estimate WSI. One of the main
456 advantages of using pore network modelling is that it is not only useful for WSI (including
457 hysteresis) but also for estimating liquid permeability and vapour diffusivity of cementitious
458 materials. Hence, the proposed work is a promising approach to address many hydraulic
459 parameters for moisture transport studies within a single framework.

460 Finally, it is acknowledged that there are shortcomings in the models used in the proposed
461 framework. For instance, uncertainties associated with the chosen cement hydration kinetics
462 model, the missing pore size distribution because of the limitation of model resolution of the
463 cement hydration kinetics model and the applicability of Jennings-Tennis's model for arbitrary
464 OPC based materials.

465

ACKNOWLEDGEMENTS

The first author gratefully acknowledges PhD sponsorship offered by SCK•CEN Academy. The findings and conclusions in this paper are those of the authors and do not represent the official position of SCK•CEN.

List of Tables

Table 1. Materials studied (CP: cement paste; M: Mortar; Co: concrete).

Table 2. Results from VCCTL and Jennings-Tennis's hydration model (CP: cement paste, Co: concrete, M: Mortar): All % values are rounded.

Table 3. R2 (coefficient of determination) values for the predicted desorption curves.

Table 1. Materials studied (CP: cement paste; M: Mortar; Co: concrete).

Material	C_3S	C_2S	C_3A	C_4AF	W/C	Aggregate/Cement	Experimental conditions	Experimental technique
CP1	56.5	18	6.3	11.4	0.45	-	Immersion in limewater for 56 days	Drying progressively for 270 days using ASTM C157, T=25 ± 0.2
CP2	57.28	23.98	3.3	7.6	0.34	-	1 year old specimen without water exchange, vacuum rewetted for drying	Drying controlled by saturated salt solutions, T=21±0.5°C
CP3	44.61	37.14	10.56	7.7	0.35	-	Endogenous curing conditions for 1 year	Drying controlled by saturated salt solutions, T=20°C
CP4	65.84	22.72	3.25	8.19	0.45	-	Same as CP3	Same as CP3
CP5	17.53	54.67	13.4	14.4	0.5	-	Immersion in limewater for 5 months	Climatic chamber, T=20±1 °C
CP6	17.53	54.67	13.4	14.4	0.8	-	Same CP5	Same CP5
M1	62.74	17.39	7.92	11.95	0.5	3.03	Same as CP3	Same as CP3
M2	17.53	54.67	13.4	14.4	0.5	3	Same as CP5	Same as CP5
M3	17.53	54.67	13.4	14.4	0.8	3	Same as CP5	Same as CP5
Co1	74.27	9.66	0.74	15.33	0.45	4.5	Same as CP3	Same as CP3
Co2	32.43	44.54	12.39	10.55	0.40	4.46	Same as CP3	Same as CP3

Table 2. Results from VCCTL and Jennings-Tennis's hydration model (CP: cement paste, Co: concrete, M: Mortar): All % values are rounded.

Material	W/C	C-S-H in cement paste (%)	HD C-S-H in C-S-H gel (%)	LD C-S-H in C-S-H gel (%)	HD C-S-H Porosity (%)	LD C-S-H Porosity (%)	Capillary Porosity (%)
CP1	0.40	51	54	46	7	9	21
CP2	0.34	45	64	36	7	6	10
CP3	0.35	45	70	30	8	5	15
CP4	0.45	44	40	60	4	10	25
CP5	0.5	47	28	72	3	13	37
CP6	0.8	49	22	78	3	14	47
M1	0.5	40	28	72	3	11	25
M2	0.5	44	28	72	3	12	16
M3	0.8	39	28	72	3	10	18
Co1	0.45	40	42	58	4	9	10
Co2	0.40	45	43	57	5	9	14

Table 3. R^2 (coefficient of determination) values for the predicted desorption curves.

Material	R^2 value
CP1	0.94
CP2	0.88
CP3	0.92
CP4	0.95
CP5	0.92
CP6	0.95
M1	0.94
M2	0.92
M3	0.94
Co1	0.93
Co2	0.85

List of Figures

Figure 1. Typical pore size distribution of cementitious materials.

Figure 2. Proposed multiscale framework for estimating water sorption isotherm.

Figure 3. Particle packing and globule concept from Jennings model

Figure 4. Comparison of pore size distribution obtained from the 3D particle packing model used in this study against the 3D particle packing model of Liu et al. [28]*: (a) HD C-S-H, and (b) LD C-S-H.*

Figure 5. Effect of different coordination numbers on a cubic network with 27 pores. a) coordination number = 6, b) coordination number = 12, c) coordination number = 26.

Figure 6. The relationship between throat diameter and its neighbouring pores.

Figure 7. Illustration of merging of different networks

Figure 8. Illustration of WSI for HD C-S-H, LD C-S-H and homogenized C-S-H gel.

Figure 9. An illustration of simulation of free drying: (a) free drying of cement paste, (b) representative pore network invaded from all the sides, (c) sequences of the invasion of moist air into a cubical hardened cement paste from all the sides with random drying path

Figure 10. Comparison of drainage curves for networks with different volume fraction of capillary pores and four different mean capillary pore sizes. (a) 40% capillary pore, (b) 50% capillary pore, (c) 60% capillary pore, and (d) 70% capillary pore.

Figure 11. Experimental observations vs. simulation using the pore network model. (a) CP1, (b) CP2, (c) CP3, (d) CP4,(e) CP5 and (f) CP6.

Figure 12. Experimental observations vs. simulation using the pore network model. (a) M1, (b) M2

Figure 13. Experimental observations vs. simulation using the pore network model. (a) Co1, and (b) Co2.

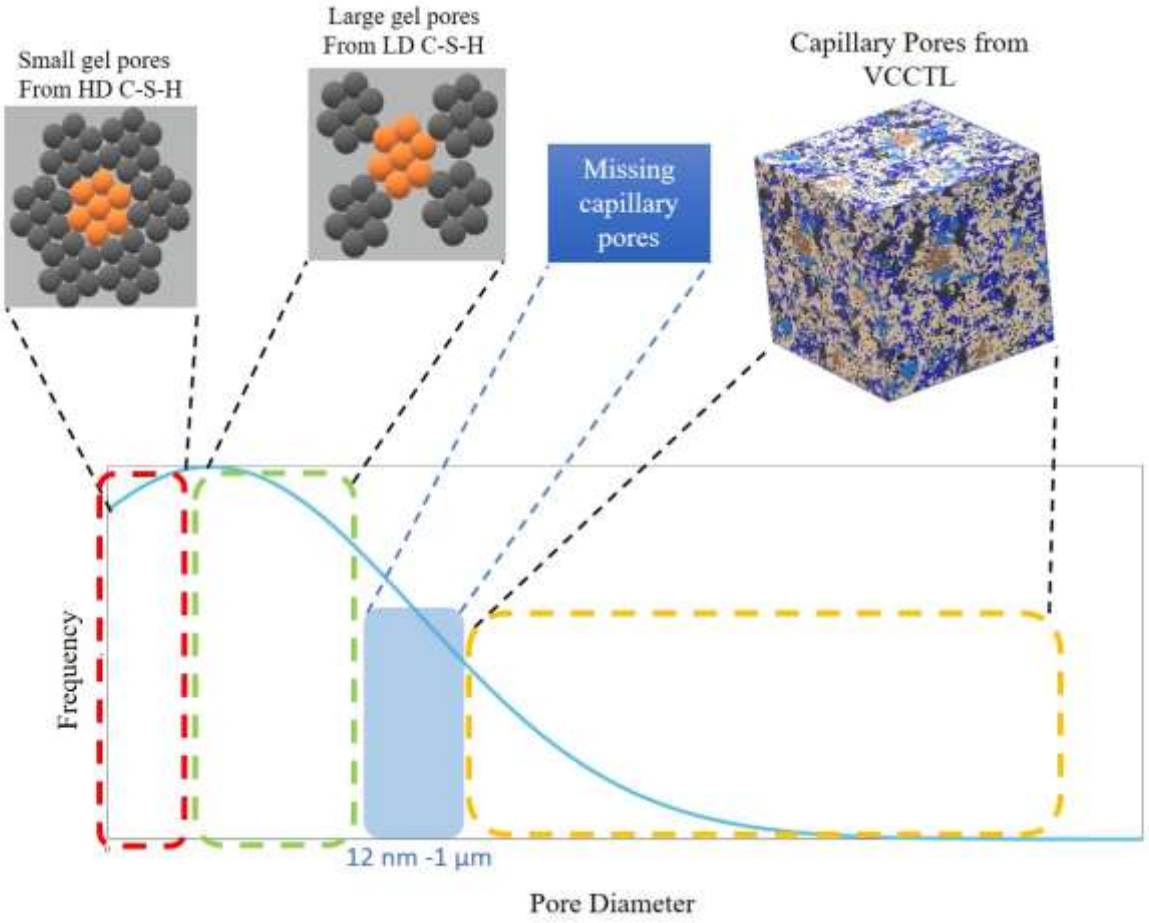

Figure 1. Typical pore size distribution of cementitious materials.

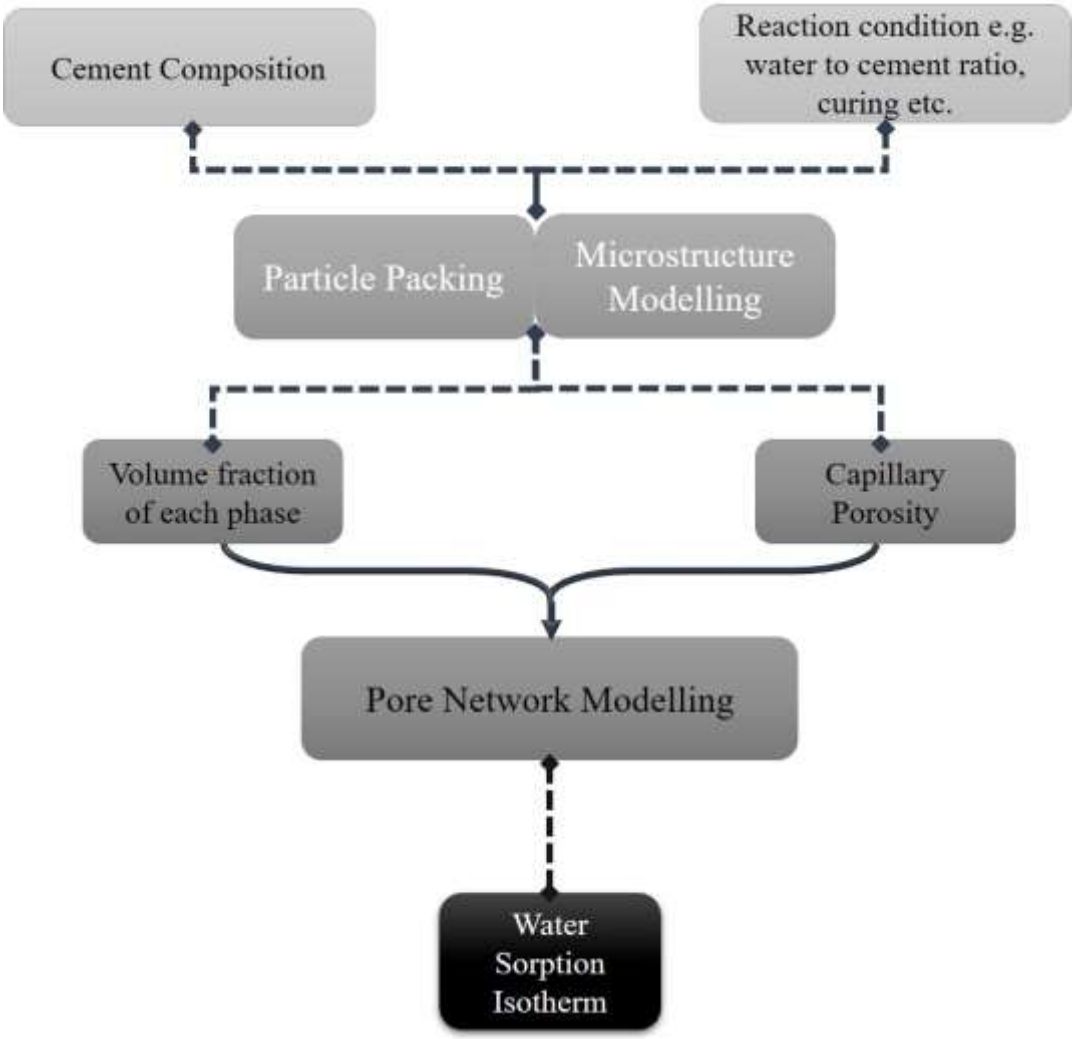

Figure 2. Proposed multiscale framework for estimating water sorption isotherm.

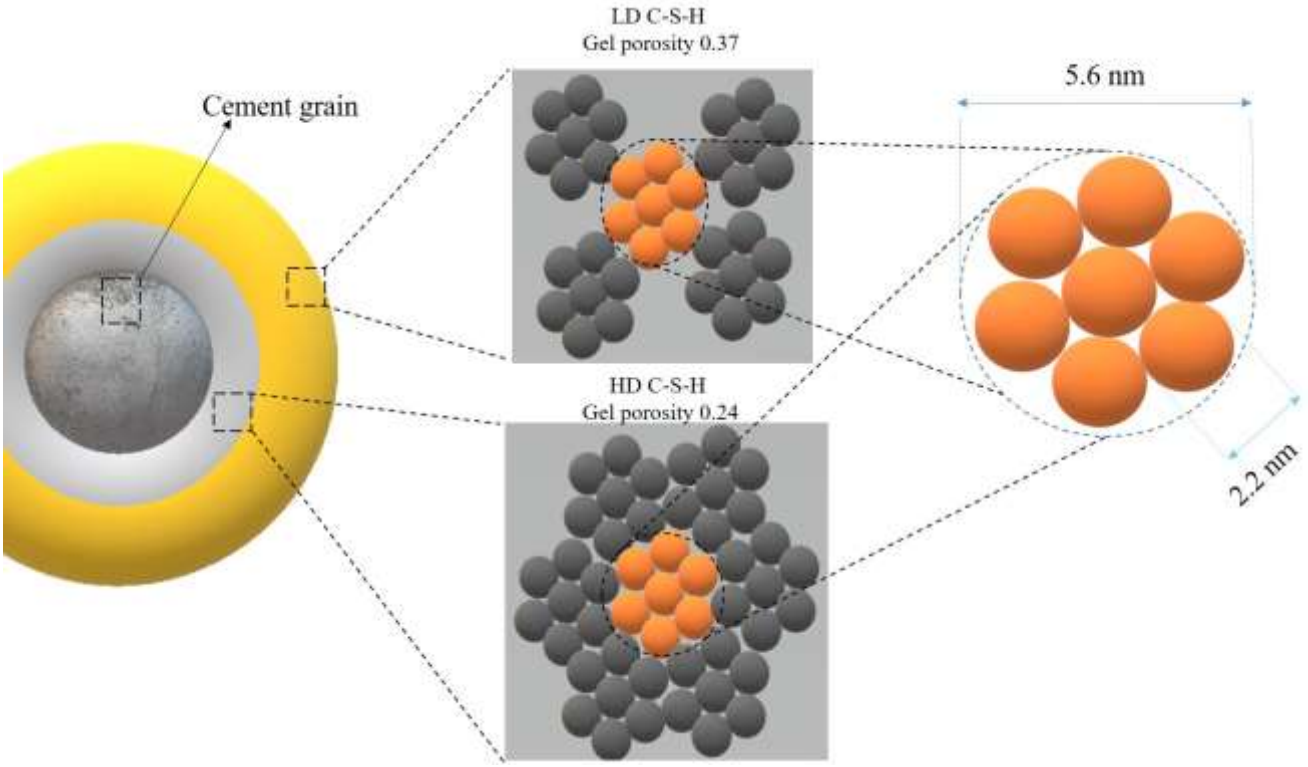

Figure 3. Particle packing and globule concept from Jennings model [20].

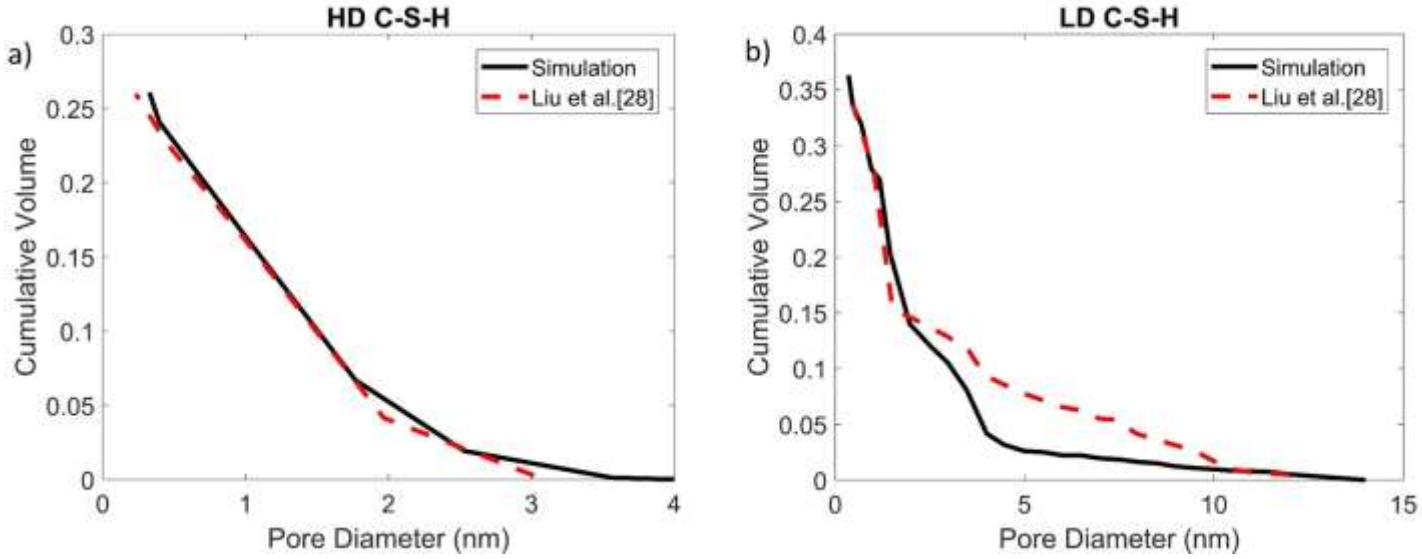

Figure 4. Comparison of pore size distribution obtained from the 3D particle packing model used in this study against the 3D particle packing model of Liu et al. [28]*: (a) HD C-S-H, and (b) LD C-S-H.*

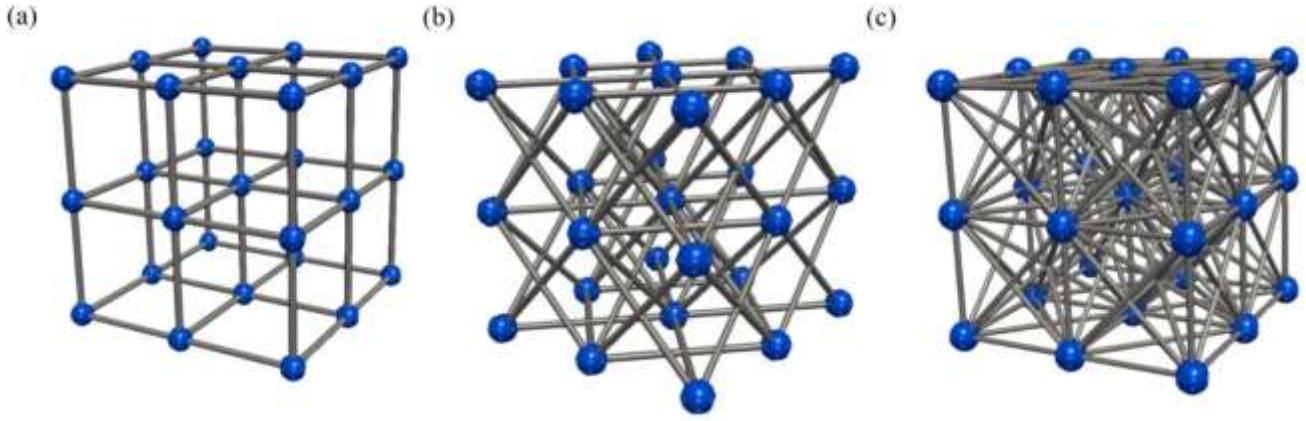

Figure 5. Effect of different coordination numbers on a cubic network with 27 pores. a) coordination number = 6, b) coordination number = 12, c) coordination number = 26.

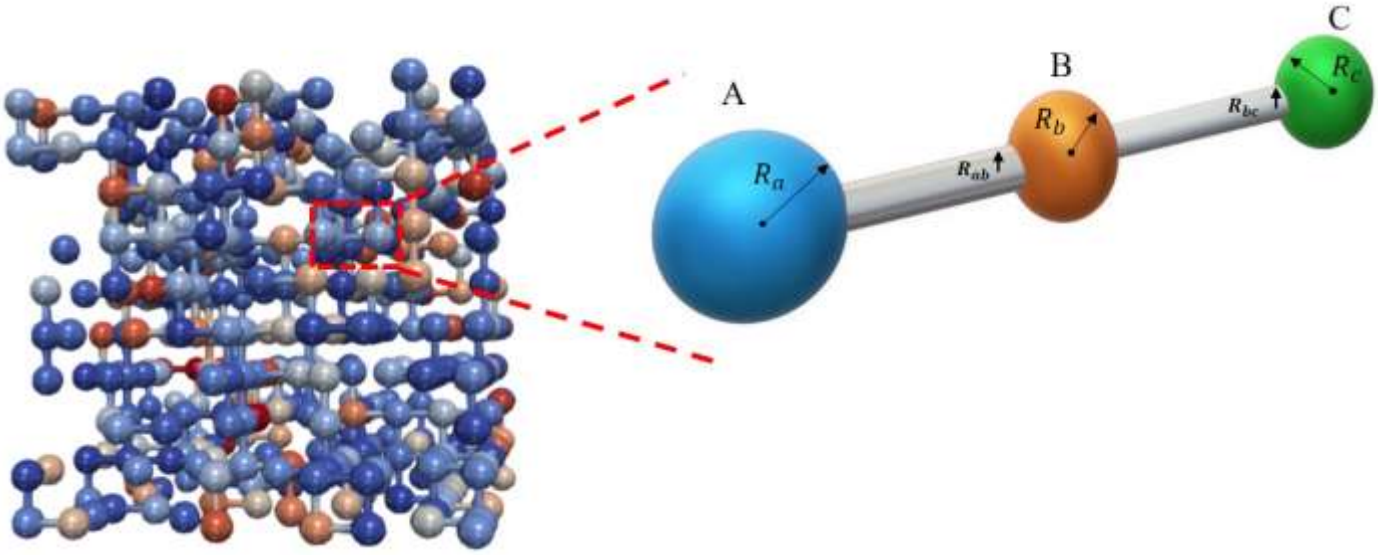

Figure 6. The relationship between throat diameter and its neighbouring pores.

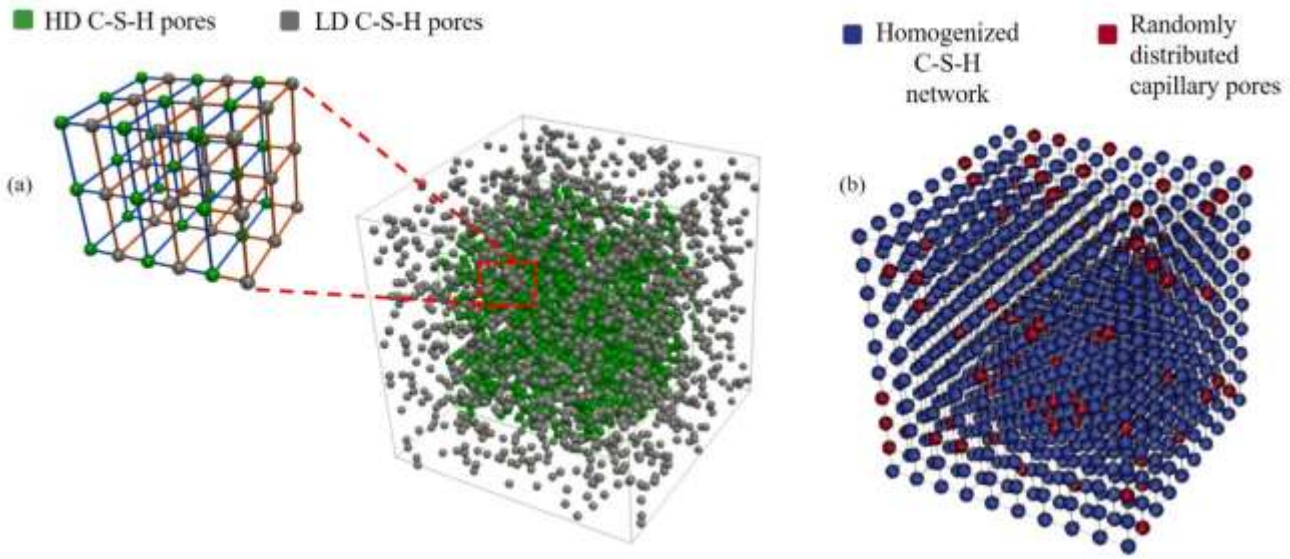

Figure 7. Illustration of merging of different networks (throats are shown for better visibility of merging process): (a) Homogenization of C-S-H gel network - merging HD C-S-H pores (green) with LD C-S-H network (grey), (b) Final network including homogenized C-S-H network (Blue) and randomly distributed capillary pores (red).

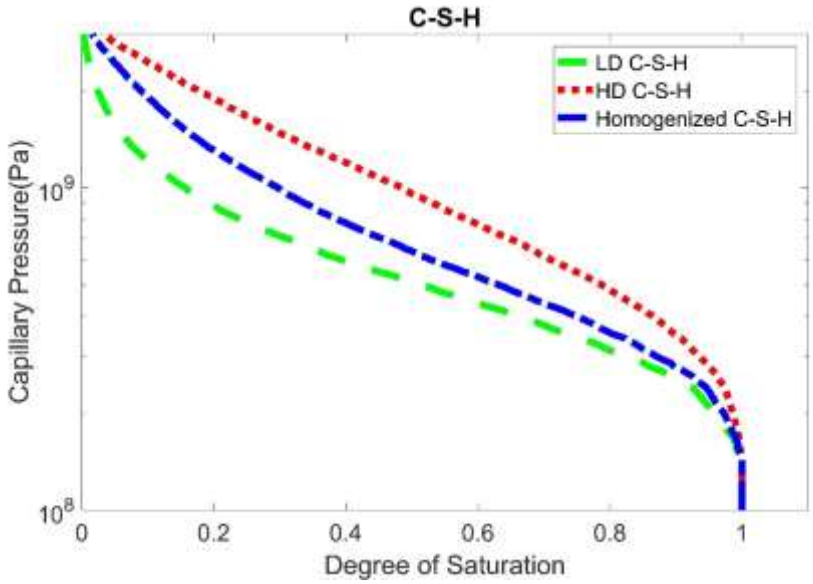

Figure 8. Illustration of WSI for HD C-S-H, LD C-S-H and homogenized C-S-H gel.

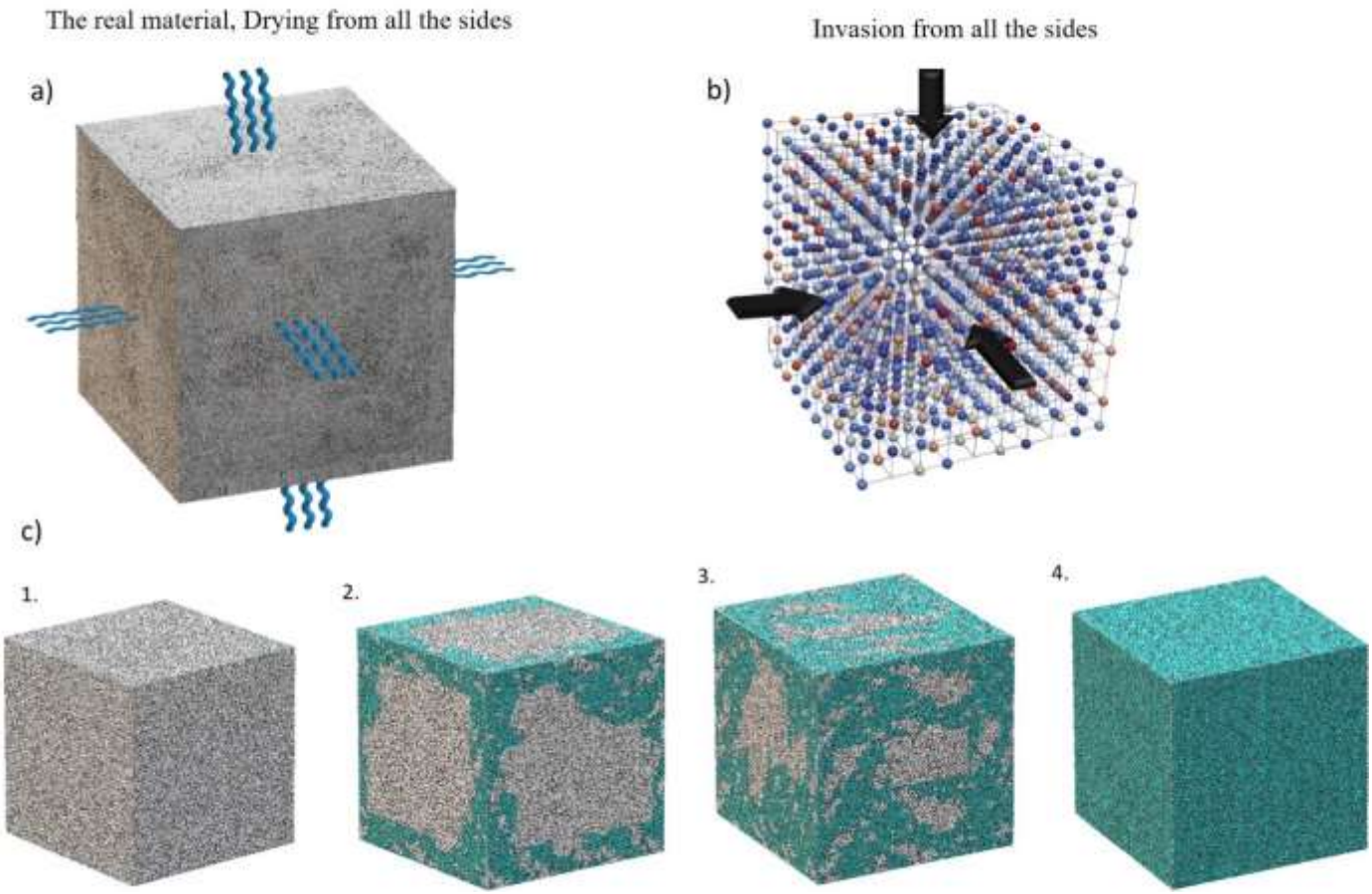

Figure 9. An illustration of simulation of free drying: (a) free drying of cement paste, (b) representative pore network invaded from all the sides, (c) sequences of the invasion of moist air into a cubical hardened cement paste from all the sides with random drying paths (from 1 as not invaded to 4 as fully invaded)

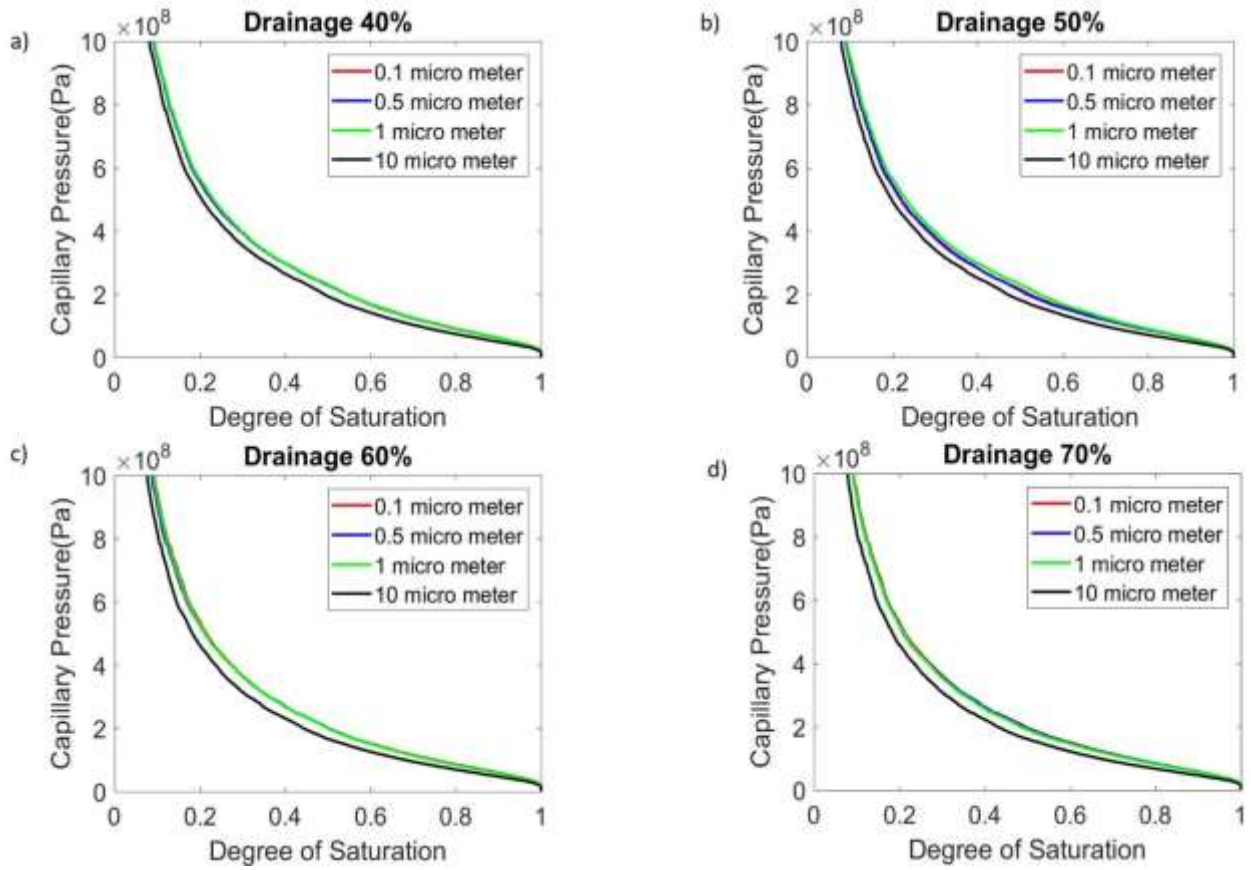

Figure 10. Comparison of drainage curves for networks with different volume fraction of capillary pores and four different mean capillary pore sizes. (a) 40% capillary pore, (b) 50% capillary pore, (c) 60% capillary pore, and (d) 70% capillary pore.

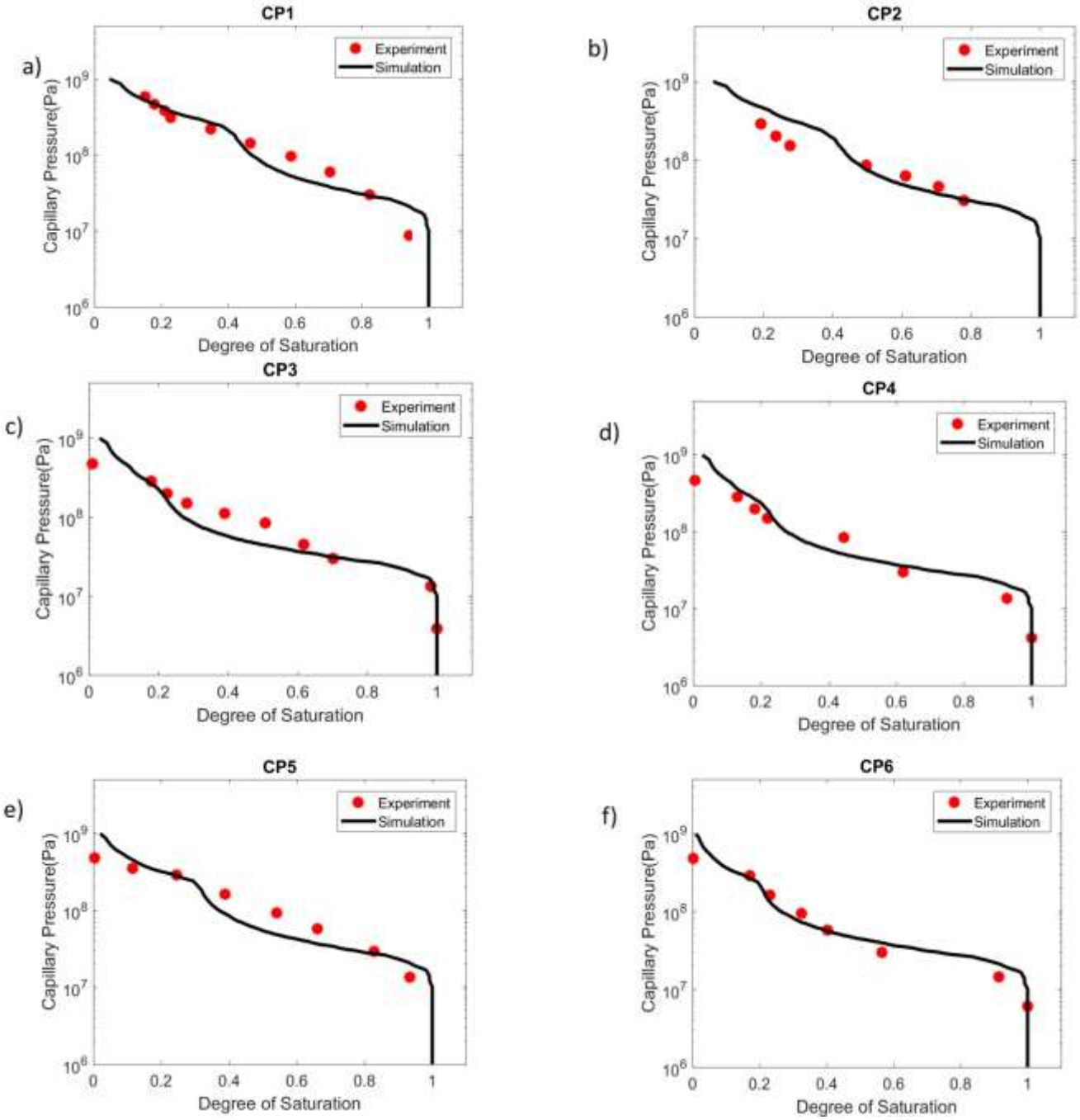

Figure 11. Experimental observations vs. simulation using the pore network model. (a) CP1, (b) CP2, (c) CP3, (d) CP4,(e) CP5 and (f) CP6.

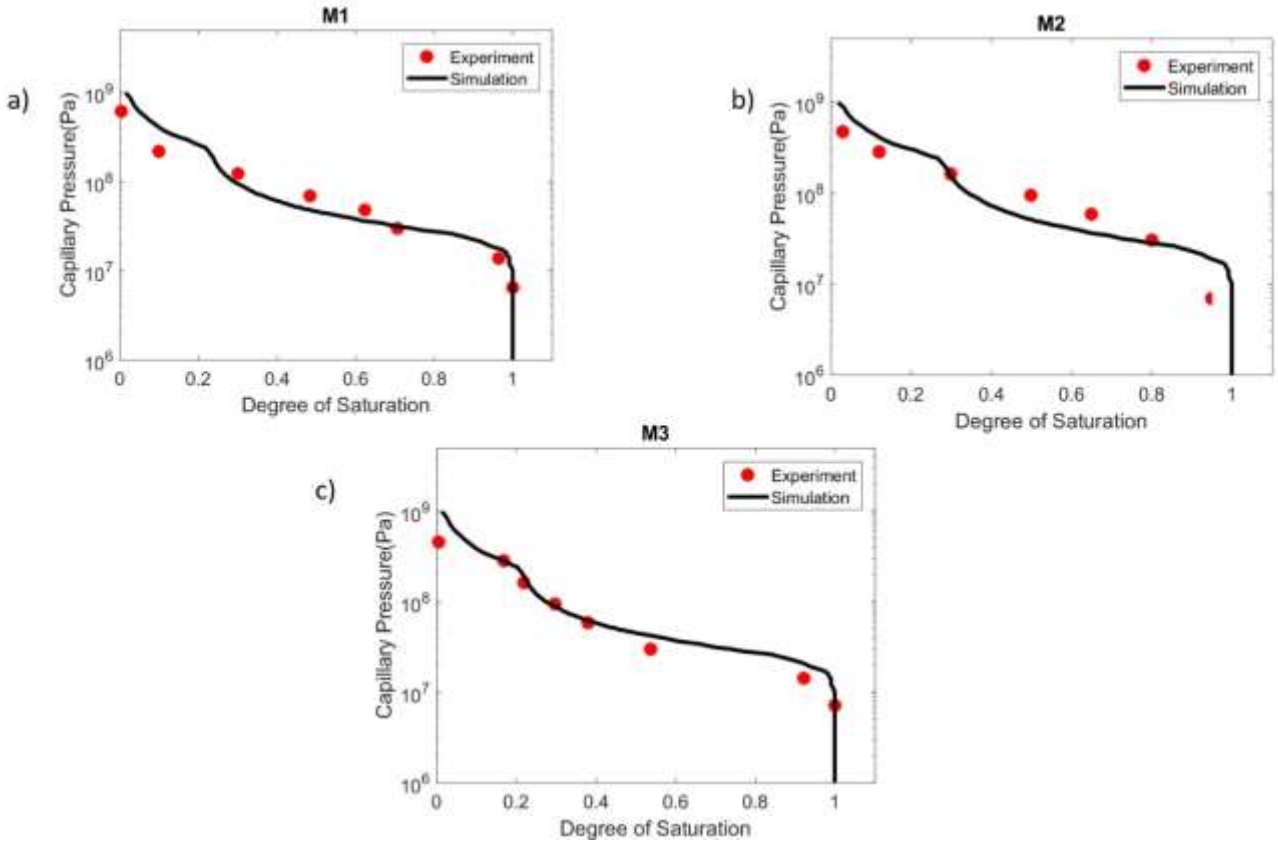

Figure 12. Experimental observations vs. simulation using the pore network model. (a) M1, (b) M2, (c) M3.

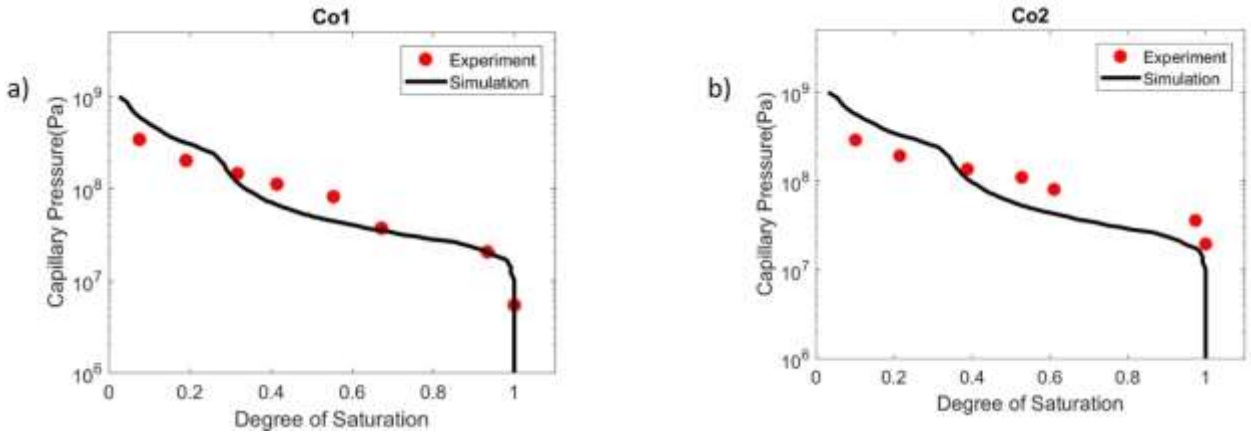

Figure 13. Experimental observations vs. simulation using the pore network model. (a) Co1, and (b) Co2.

REFERENCES

1. Zdeněk P. Bažant and M. Jirásek, *Creep and Hygrothermal Effects in Concrete Structures.* Springer Netherlands, 2018. **Series Volume 225**.
2. Zdeněk P. Bažant, et al., *Microprestress-Solidification Theory for Concrete Creep. I: Aging and Drying Effects.* Journal of Engineering Mechanics, 1997. **123**(11).
3. Tanabe T., et al., *Creep, Shrinkage and Durability Mechanics of Concrete and Concrete Structures.* (Japan, CRC 2009), 2009. **Vol 1**(1st Edn).
4. Baroghel-Bouny V., *Water vapour sorption experiments on hardened cementitious materials: Part I: Essential tool for analysis of hygral behaviour and its relation to pore structure.* Cement and Concrete Research, 2007(37): p. 414-437.
5. De Burgh J.M. and Foster S.J., *Influence of temperature on water vapour sorption isotherms and kinetics of hardened cement paste and concrete.* Cement and Concrete Research, 2017. **92**: p. 37-55.
6. Zhang Z., Thiery M., and Baroghel-Bouny V., *An equation of drying kinetics for cementitious materials.* Drying Technology, 2017. **36**(12): p. 1-14.
7. Wu M., Johannesson B., and Geiker M., *A study of the water vapor sorption isotherms of hardened cement pastes: Possible pore structure changes at low relative humidity and the impact of temperature on isotherms.* Cement and Concrete Research, 2014. **56**: p. 97-105.
8. Reatto A., *Validity of the Centrifuge Method for Determining the Water Retention Properties of Tropical Soils.* 2008. **72**(6): p. 1547-1553.
9. Reis R.M., *Determination of the Soil-Water Retention Curve and the Hydraulic Conductivity Function Using a Small Centrifuge.* Geotechnical Testing Journal, 2011. **34**(5): p. 457-466.
10. Thomas Rougelot, Frédéric Skoczylas, and Nicolas Burlion, *Water desorption and shrinkage in mortars and cement pastes: Experimental study and poromechanical model.* Cement and Concrete Research, 2009. **39**: p. 36–44.
11. James M. de Burgh, Stephen J. Foster, and H.R. Valipour, *Prediction of water vapour sorption isotherms and microstructure of hardened Portland cement pastes.* Cement and Concrete Research, 2016. **81**(134): p. 134-150.
12. Aditya Kumar, et al., *Water Vapor Sorption in Cementitious Materials Measurement, Modeling and Interpretation.* Transport in Porous Media, 2014. **103**(1): p. 69-98.
13. Matthew B. Pinson, Enrico Masoero, and Hamlin M. Jennings, *Hysteresis from Multiscale Porosity: Modeling Water Sorption and Shrinkage in Cement Paste.* American Physical Society, 2015. **3**.
14. Torben C. Hansen, *Physical structure of hardened cement paste. A classical approach.* Materials and Structures, 1986. **19,**(6): p. 423–436.
15. Enrico Masoero, Gianluca Cusatis, and G.D. Luzio, *C–S–H gel densification: The impact of the nanoscale on self-desiccation and sorption isotherms.* Cement and Concrete Research, 2018. **109**: p. 103-119.
16. Mason G., *A model of adsorption-desorption hysteresis in which hysteresis is primarily developed by the interconnections in a network of pores.* Proceedings of the Royal Society of London, 1983. **390:**: p. 47–72.
17. Islahuddin M. and Janssen H., *Hygric property estimation of porous building materials with multiscale pore structures.* Energy Procedia, 2017. **132**: p. 273-278.
18. Constantinides G. and Ulm F.J., *The effect of two types of C-S-H on the elasticity of cement-based materials: Results from nanoindentation and micromechanical modeling.* Cement and Concrete Research, 2004. **34**(1): p. 67-80.
19. Fonseca P.C., Jennings H.M., and Andrade J.E., *A nanoscale numerical model of calcium silicate hydrate.* Mechanics of Materials, 2011. **43**: p. 408–419.

20. Jennings, H.M., *A model for the microstructure of calcium silicate hydrate in cement paste.* Cement and Concrete Research, 2000. **30** (1): p. 101-116.
21. Ulm F.J., Constantinides G., and Heukamp F.H., *Is concrete a poromechanics material? – A multiscale investigation of poroelastic properties.* Mater Struct, 2004. **37**: p. 43-58.
22. Jennings H.M., et al., *A multi-technique investigation of the nanoporosity of cement paste.* Cem Concr Res, 2007. **37**: p. 329-336
23. Thomas J.J. and Jennings H.M., *A colloidal interpretation of chemical aging of the C-S-H gel and its effects on the properties of cement paste.* Cem Concr Res, 2006. **36**: p. 30-38.
24. Jaeger H.M. and Nagel S. R., *Physics of granular state.* Science,, 1992. **255**(5051): p. 1523-1531.
25. Sloane N. J. A., *Kepler's conjecture confirmed.* Nature, 1998. **395**: p. 435-436.
26. Donev A., et al., *Improving the density of jammed disordered packings using ellipsoids.* Science, 2004. **303**: p. 990-993.
27. Georgios Constantinides, *Invariant Mechanical Properties of Calcium-Silicate-Hydrates (C-S-H) in Cement-Based Materials: Instrumented Nanoindentation and Microporomechanical Modeling.* MASSACHUSETTS INSTITUTE OF TECHNOLOGY, 2006.
28. Lin Liu, et al., *Numerical modeling of drying shrinkage deformation of cement-based composites by coupling multiscale structure model with 3D lattice analyses.* Computers and Structures 2017. **178**: p. 88–104.
29. Thomas J.J., et al., *Modeling and simulation of cement hydration kinetics and microstructure development.* Cement and Concrete Research, 2011. **41**(12): p. 1257-1278.
30. Bullard J.W., *VCCTL Version 9.5 User Guide.* NIST, 2014.
31. Van Breugel K., *Simulation of hydration and formation of structure in hardening cement-based materials.* TU Delft, 1991.
32. Ye, G., *Experimental Study and Numerical Simulation of the Development of the Microstructure and Permeability of Cementitious Materials.* Delft University of Technology, 2003.
33. Li, K., *Numerical Determination of Permeability in Unsaturated Cementitious Materials.* Delft University of Technology, 2017.
34. Gostick J., Aghighi M., and Hinebaugh J., *OpenPNM: A Pore Network Modeling Package.* Computing in Science & Engineering, 2016. **18**(4): p. 60-74.
35. Raoof A., *PoreFlow: A Complex Pore-Network Model for Simulation of Reactive Transport in Variably Saturated Porous Media.* Computers & Geosciences, 2013. **61**: p. 160-174.
36. Jennings H.M. and Tennis P.D., *A model for the developing microstructure in Portland cement pastes.* frAmer. Ceram. Soc, 1994. **77**(12): p. 3161-3172.
37. P. Kumar Mehta and Paulo J. M. Monteiro, *Concrete: Microstructure, Properties, and Materials.* McGraw Hill Professional, 2013.
38. David Wilkinson and Jorge F Willemsen, *Invasion percolation: a new form of percolation theory.* Journal of Physics A: Mathematical and General, 1983. **16** p. 3365-3376. .
39. MASON G., *A Model of the Pore Space in a Random Packing of Equal Spheres* Journal of Colloid and Interface Science, 1971. **35**(2): p. 279-287.
40. Arne Hillerborg, *A modified absorption theory.* Cement and Concrete Research, 1985. **15**(5): p. 809-816.
41. Baroghel-Bouny V. and Godin J., *Experimental study on drying shrinkage of ordinary and high-performance cementitious materials.* RILEM Conf Shrinkage, 2001. **3**: p. 13-22.
42. Baroghel-Bouny V., et al., *Characterization and identification of equilibrium and transfer moisture properties for ordinary and high-performance cementitious materials.* Cement and Concrete Research, 1999. **29**: p. 1225–1238.

43. Ranaivomanana H., et al., *Toward a better comprehension and modeling of hysteresis cycles in the water sorption–desorption process for cement based materials.* Cement and Concrete Research 2011. **41**: p. 817-827.
44. Galen Egan, et al., *Re-examining the influence of the inclusion characteristics on the drying shrinkage of cementitious composites.* Construction and Building Materials, 2017. **146**: p. 713-722.
45. Baroghel-Bouny V., et al., *Characterization and identification of equilibrium and transfer moisture properties for ordinary and high-performance cementitious materials.* Cement and Concrete Research 1999. **29** p. 1225–1238.
46. Vlahinić Ivan, Jennings Hamlin M., and Thomas Jeffrey J., *A constitutive model for drying of a partially saturated porous material.* Mechanics of Materials, 2009. **41**(3): p. 319-328.
47. Hughes A. and Grawoig D., *Statistics: A Foundation for Analysis.* Addison-Wesley Educational Publishers Inc, 1971.